Journal of Materials Chemistry A

ROYAL SOCIETY OF CHEMISTRY

PAPER

View Article Online
View Journal | View Issue

Cite this: J. Mater. Chem. A, 2025, 13, 36341

Diamondoid-templated lithium single-cation conduction in solid-state organic electrolytes

Jack McAlpine,[a] Michael Rebarchik,[a] Hrishikesh Tupkar,[a] Zhen Jiang,[a] Sila Alemdar,[a] Marissa Gallmeyer,[a] Jeremy E. Dahl,[b] Robert M. K. Carlson,[b] Boryslav O. Tkachenko,[cd] Heike Hofstetter,[e] Catherine F. M. Clewett,[e] Peter R. Schreiner,[cd] Whitney S. Loo,[a] Manos Mavrikakis[a] and Matthew A. Gebbie *[a]

Rapid growth in battery use increases the focus on battery safety and sustainability. While ionic liquids and organic ionic plastic crystals show promise as safe battery electrolytes, they often exhibit poor lithium transport due to excessive lithium-anion coordination and preferential organic ion conduction. We show that adamantane can be leveraged to hinder organic cation motion while templating lithium transport pathways to enable solid-state lithium single-cation conduction. By using solid-state NMR spectroscopy to study anion conformational changes and electrochemical impedance spectroscopy to evaluate lithium mobility in adamantane and diamantane salts, we reveal that adamantane-templated assembly of anion networks is key for enabling lithium-ion mobility. Further, we find that solid-state conductivity is a strong function of lithium concentration, rising two orders of magnitude at room temperature upon increasing lithium from 5 to 15 mol percent. Our experimental findings are substantiated by density functional theory computations, where we determine the lowest-energy transport pathway guiding lithium transport within the adamantane-templated salt. Together, temperature-dependent conductivity measurements, solid-state NMR spectroscopy, pulsed gradient spin echo (PGSE) NMR spectroscopy and electronic structure calculations establish that lithium is the only mobile cation in the solid electrolyte phase, as adamantyl groups completely inhibit organic cation motion. Hence, our findings show that lithium transport occurs within dynamic bis(trifluoromethanesulfonyl)imide (TFSI) channels within the diamondoid templated electrolyte, achieving conductivities exceeding 0.1 mS cm^{-1} at 70 °C. This demonstrates that diamondoid-derived electrolytes show promise as organic lithium single-cation conductors that can address longstanding battery performance challenges associated with low lithium transference in conventional ionic liquid and polymeric electrolytes.

Received 28th April 2025
Accepted 12th September 2025

DOI: 10.1039/d5ta03373j

rsc.li/materials-a

Introduction

Increased battery use has drawn focus to the safety concerns of lithium-ion battery materials, most notably battery fires fueled by flammable organic solvents.[1,2] To improve safety, electrolytes are being developed using organic salts as the solvent for lithium instead of organic carbonates.[3–5] These salt electrolytes are nonflammable and highly stable, hindering decomposition and catastrophic battery failure. Though typically thought of as crystalline solids, salts composed of charge-dispersed ions that do not readily form crystalline lattices can result in materials like ionic liquids or organic ionic plastic crystals. While ionic liquids and organic plastic ionic crystals have been under extensive investigation for use as battery electrolytes,[6–9] low lithium mobility and lithium transference have been challenges facing translation of ionic liquid-derived electrolytes into commercial devices.[10–13]

In particular, lithium is a small, charge-dense cation that exhibits strong electrostatic coordination with organic anions.[14] For example, addition of lithium cations to conventional ionic liquids often causes electrolyte conductivity to decrease.[15–19] One proposed reason for the reduced conductivity is stronger ionic interactions between lithium ions and anions than between organic cations and anions. Not only do these interactions increase viscosity,[15] but can create ionic clusters of

[a]Department of Chemical and Biological Engineering, University of Wisconsin–Madison, 1415 Engineering Drive, Madison, Wisconsin 53706, USA. E-mail: gebbie@wisc.edu

[b]Materials Science and Engineering, Stanford University, Stanford, California 94305, USA

[c]Institute of Organic Chemistry, Justus Liebig University, Heinrich-Buff-Ring 17, 35392 Giessen, Germany

[d]Center for Materials Research, Justus Liebig University, Heinrich-Buff-Ring 16, 35392 Giessen, Germany

[e]Department of Chemistry, University of Wisconsin–Madison, Madison, Wisconsin 53706, USA

multiple anions coordinated to a single lithium ion, preventing lithium ion transport.[13]

Notably, for ionic liquids and other electrolytes where high ion concentrations drive the formation of ionic networks, lithium mobility and transport can be largely decoupled from the total conductivity, which is often defined by the motion of weakly coordinated organic ions. For example, many experiments and simulations show that the primary current carrier in ionic liquid-lithium salt mixtures is not lithium ions. Rather, the salt cations and anions not involved in ionic clusters are the primary current carriers.[11,13,20] Thus, the measured conductivity overvalues the efficacy of the electrolyte for battery operation. Ultimately, control over which ionic species is most mobile in these systems is highly desired to produce the most effective battery electrolyte.

An ideal organic salt electrolyte would allow for preferential lithium-ion conduction, which could originate from suppression of lithium-anion coordination and hindering motion of the surrounding organic ion network while still allowing for thermally activated lithium motion. Previously, we showed that functionalizing ionic liquid cations with diamondoid moieties can immobilize organic cations in ionic liquids *via* strong London dispersion interactions[21,22] between entropically constrained hydrocarbon clusters, while still maintaining local lithium mobility.[23]

Diamondoids are hydrocarbon molecular clusters, where carbon atoms are present in diamond-like sp^3 bonding.[24] Diamondoids can range in size from $C_{10}H_{16}$, called adamantane, up to clusters that have tens of carbon atoms, and these higher diamondoids can exhibit a wide range of structures with all diamondoids with more than three adamantane exhibiting constitutional isomers.[21,25,26] Unlike conventional linear and cyclic hydrocarbons, polycyclic diamondoids are three-dimensionally rigid, which drastically decreases the entropic penalty associated with pairwise assembly.[27,28] Diamondoids can also exhibit uniquely strong dispersion interactions,[29] which, together with lowered conformational entropy, provides new ways to tune ionic liquid nanostructure and assembly. For example, we previously showed that diamondoids can be leveraged to template organic ionic plastic crystal phases with defined cationic networks, which concurrently templates bis(trifluoromethanesulfonyl)imide (TFSI) anions into molecular level channels that appeared to be conducive for lithium ion conduction.[23]

In this work, we show that the size and orientation of the diamondoid attachment to the cation changes the conformation and assembly of anion networks with concurrent changes to lithium mobility. By comparing 1-(adamant-1-yl)-3-methylimidazolium (AdImMe), 1-(diamant-1-yl)-3-methylimidazolium (Diam-1-ImMe), or 1-(diamant-4-yl)-3-methylimidazolium (Diam-4-ImMe) cations paired with the TFSI anion, we observed different anion conformations using solid-state NMR spectroscopy, highlighting how the diamondoid functional group acts as a structure directing agent for templating the electrolyte nanostructure. TFSI mainly exists in either the *cis* or *trans* conformer (Fig. 1).[30] In solid phases exhibiting weak cation–anion interactions, TFSI has been reported to adopt the *trans* conformer when paired with organic cations and in the presence of metal cations, a mixture of *cis* and *trans* conformers.[31–34] A mixture of *cis* and *trans* TFSI conformers are also present in neat ionic liquids.[34] In prior work we observed that using adamantane as the diamondoid moiety results in TFSI that is neither *cis* nor *trans*; instead, the anion is in a twisted *gauche* conformation.[23] The preferred structure of TFSI and lithium ions in ionic liquid solutions is bidentate coordination from two different TFSI anions.[35,36] With the TFSI anions being neither *cis* nor *trans*, TFSI ions may not be able to perform bidentate coordination.

Yet to this point, evidence of long-range lithium-ion conduction and information about ion transport mechanisms in these diamondoid-derived electrolytes was lacking. In this work, we designed and tested three different diamondoid salts, [AdImMe][TFSI], [Diam-1-ImMe][TFSI], and [Diam-4-ImMe][TFSI], and show that these different diamondoid substituents template organic phases with different TFSI conformers (Fig. 1). These conformers are *cis*, *gauche*, and *trans*. Using electrochemical impedance spectroscopy (EIS), we evaluated the temperature-dependent conductivity of these diamondoid

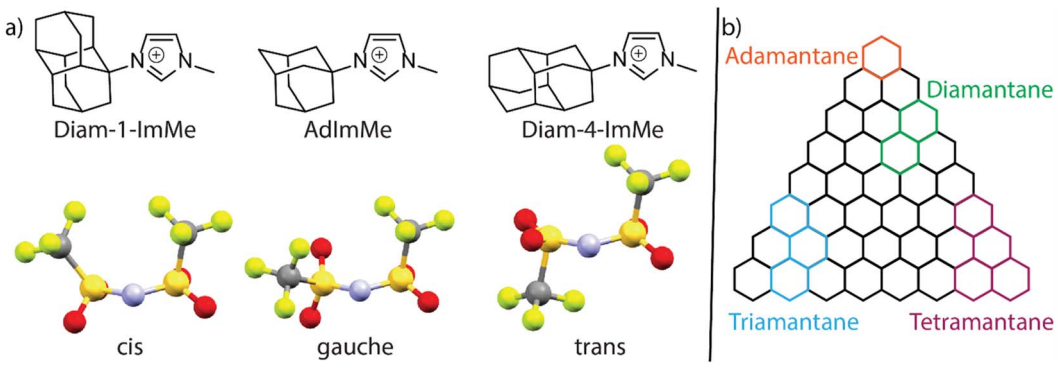

Fig. 1 (a) The three diamondoid cations tested, 1-(diamant-1-yl)-3-methylimidazolium (Diam-1-ImMe), 1-(adamant-1-yl)-3-methylimidazolium (AdImMe), and 1-(diamant-4-yl)-3-methylimidazolium (Diam-4-ImMe). The corresponding conformer of bis(trifluoromethanesulfonyl)imide (TFSI) present in the neat salt is shown below each diamondoid cation. (b) Visualization of how diamondoids can be cut from a diamond lattice. The following color scheme was used for atoms: N – light blue, O – red, S – yellow, C – dark grey, F – light green.

electrolytes with different concentrations of [Li][TFSI]. To gain mechanistic insight, density functional theory (DFT) computations were performed to identify potential Li-ion conduction pathways through diamondoid salts and shed light on how the modified anion conformer may impact lithium mobility. By defining ionic structure to minimize interaction with lithium ions, we demonstrate a design paradigm for solid-state electrolytes with improved lithium single-ion conduction.

Results

Evaluating anion conformation

Previously, we studied the TFSI anion conformation of neat [AdImMe][TFSI] and [Diam-4-ImMe][TFSI] salts,[23] where we used a combination of solid-state NMR spectroscopy and single-crystal X-ray crystallography to determine that the multiple peaks in the ^{19}F NMR spectrum of [AdImMe][TFSI] result from *gauche* conformers with unsymmetric fluorine environments. Here, we report that the solid-state ^{19}F NMR data of [Diam-1-ImMe][TFSI] shows a convolution of peaks (Fig. 2). The electron density of these peaks is nearly identical, and the relative area of these peaks is 1 : 2, so it is unclear what difference in conformation exists in this structure. Previous NMR datum indicates that the TFSI anions in the [Diam-1-ImMe][TFSI] salt are likely in the *cis* conformation while the TFSI anions in the [Diam-4-ImMe][TFSI] salt are likely in the *trans* conformation.[37]

The conformational changes associated with differing fluorine environments are also exhibited in Raman modes associated with the TFSI anion. We have previously reported that the [AdImMe][TFSI] and [Diam-4-ImMe][TFSI] salts exhibit Raman modes *ca.* 745 cm^{-1} and 743 cm^{-1} respectively, with shifts in wavenumbers corresponding to TFSI conformational changes.[23]

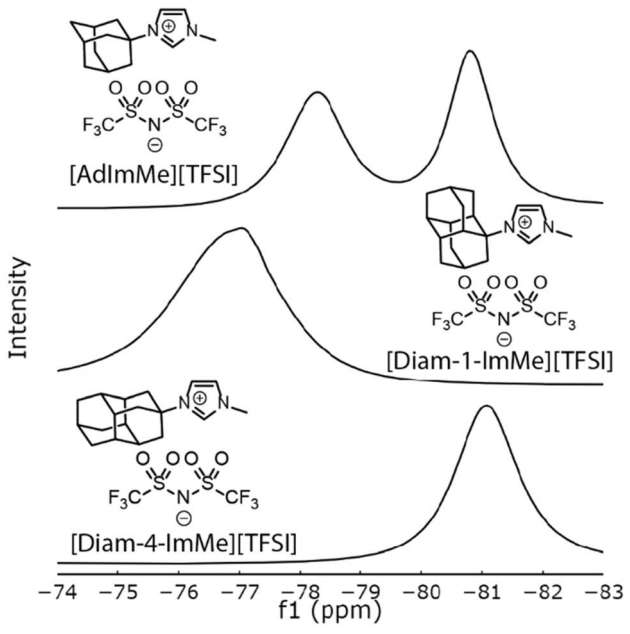

Fig. 2 Solid-state ^{19}F NMR spectra of [AdImMe][TFSI], [Diam-1-ImMe][TFSI] and [Diam-4-ImMe][TFSI].

[Diam-1-ImMe][TFSI] exhibits a TFSI stretching mode at 741 cm^{-1} (Fig. S10), suggesting the presence of a conformer that differs from AdImMe and Diam-4-ImMe containing salts.

Conductivity and activation energy

We prepared mixtures of each diamondoid salt with 10 mol% [Li][TFSI] to evaluate these materials as potential solid-state electrolytes for lithium-ion batteries. The salt mixtures were pressed into pellets with 6 mm diameters and thicknesses between 1 mm and 2 mm and placed in pouch cells. Each pellet was sandwiched between two copper discs within the pouch cell. Cell assembly is explained in detail in the Materials and methods section.

Conductivity was evaluated using EIS in a temperature range of 35–75 °C. Mixtures containing 10 mol% [Li][TFSI] with either [Diam-1-ImMe][TFSI] or [Diam-4-ImMe][TFSI] were too resistive to accurately model and evaluate conductivity until 75 °C where the conductivity was measured to be on the order of μS cm^{-1} (SI Fig. S3 and S4).

Mixtures of [Li][TFSI] and [AdImMe][TFSI] are conductive at room temperature and within the 35–75 °C range tested while neat [AdImMe][TFSI] is an electrical insulator at room temperature (SI Fig. S7). Compositions containing 5, 10, and 15 mol% [Li][TFSI] were evaluated. Fig. 3a shows the conductivity of each mixture as a function of temperature. Surprisingly the measured conductivity increases by approximately an order of magnitude with each 5% increase in the total mol% of [Li][TFSI] in the mixture, which could originate from increased disorder associated with substituting lithium cations for the much larger AdImMe cation facilitates lithium transport. The conductivity of each mixture increases by at most two orders of magnitude over the ascribed temperature range, and further investigation is under way to mechanistically understand how lithium addition modifies conductivity mechanisms.

Conductivity studies suggest that diamondoid electrolytes are competitive among some classes of solid-state electrolytes, with OIPCs exhibiting conductivities in the range of 10^{-6} to 10^{-4} S cm^{-1} and polymer electrolytes having room temperature conductivities lower than 10^{-6} S cm^{-1} at room temperature.[38,39] However, the diamondoid electrolytes exhibit lower conductivity than highly engineered ceramics like lithium lanthanum zirconium oxide (LLZO) or sodium super ionic conductors (NASICONs), which have room temperature conductivities approaching 10^{-3} S cm^{-1}.[40,41] Nevertheless, the compositional design space of diamondoid electrolytes is immense, leaving many open opportunities to further increase the conductivity of diamondoid phases to be closer to that of highly optimized ceramic materials.

$$\sigma = A\, e^{\frac{-E_a}{RT}} \quad (1)$$

To determine the apparent activation energy of the conductivity of these mixtures, eqn (1) was applied. In eqn (1) we replace k (the formal rate) with the conductivity σ (S cm^{-1}), while A (S cm^{-1}) is the Arrhenius pre-factor, T (K) the temperature, R (J mol^{-1} K^{-1}) the ideal gas constant, and E_a (J mol^{-1})

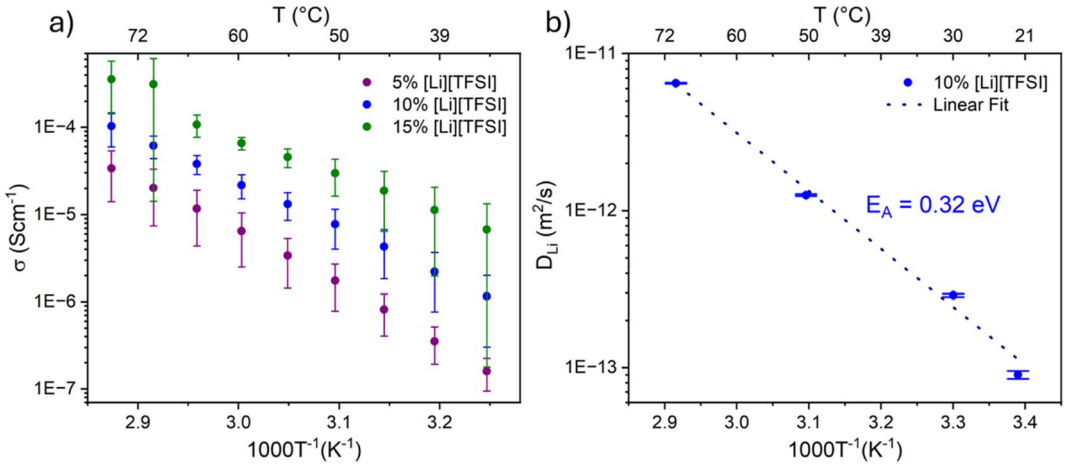

Fig. 3 (a) Conductivity *versus* temperature plots of different compositions of [Li][TFSI] with [AdImMe][TFSI], (b) Arrhenius plot from the lithium self-diffusion coefficients of the 10% [Li][TFSI] in [AdImMe][TFSI]. Error bars indicate uncertainty in measured D_{Li}.

the activation energy. There is strong agreement between the data and this model (SI Fig. S8). For [AdImMe][TFSI], the fitted activation energy decreases with increasing [Li][TFSI] mol percent with values of 1.24 eV for the 5 mol% [Li][TFSI], 1.03 eV for the 10 mol% [Li][TFSI], and 0.93 eV for 15 mol% [Li][TFSI]. While these fitted apparent activation energies are double or triple that of many common solid-state electrolytes[40,41] and ionic liquid electrolytes,[42] the diamondoid-derived electrolytes still achieve conductivity approaching technologically relevant mS cm^{-1} range at modestly elevated temperatures.

Pulsed field gradient – NMR self diffusion coefficient measurement

To investigate individual ion mobilities, we measured self-diffusion coefficients of Li^+ (D_{Li}), AdImMe (D_H), and TFSI (D_F) with pulsed field gradient (PFG) NMR (Table S3). We acquired ^1H, ^{19}F, and ^7Li spectra at room temperature and at elevated temperatures. Since only TFSI contains fluorine atoms, and only AdImMe contains hydrogen atoms, D_F and D_H were directly associated with organic anion and organic cation mobilities.

Within the maximum gradient strength of the probe, D_H was too small to be measurable, indicating limited to negligible AdImMe cation motion. PFG NMR confirms lithium cation motion within [AdImMe][TFSI] electrolytes. Surprisingly, PFG NMR also reveals that fluorine motion closely tracks that of lithium, with a ratio between D_{Li} and D_F being approximately one across the temperature range 22 – 70 °C. As a result, we conclude that either the apparent diffusion coefficient of fluorine is influenced by conformational changes of TFSI anions within TFSI domains or that Li-TFSI is exhibiting solid-state diffusion as a coordination complex. Notably, the activation energy associated with lithium diffusion is 0.32 eV, in agreement with the conductivity activation energy of other common solid-state electrolytes,[43–45] and D_{Li} reaching up to 6.50×10^{-12} m^2 s^{-1} at 70 °C. This value is comparable to single-ion conducting polymer electrolytes reported previously[46] and shows promise when further improvements in material processing are made.

DFT analysis of transport mechanisms

First-principles computations were performed to understand the mechanism of Li^+ transport through the solid-state [AdImMe][TFSI] electrolyte, which can shed light on the ionic conductivity measured in temperature-dependent EIS experiments. Stable Li^+ coordination environments were identified to propose possible diffusion paths across the [AdImMe][TFSI] unit cell. To balance computational cost and Li concentration, the electrolyte model included four ion pairs whereby the unit cell contained three $[AdImMe]^+$ cations, four $[TFSI]^-$ anions, and one Li^+ cation, corresponding to a molar concentration of $c(Li^+) = 0.25$ (see SI Fig. S1). Systematic investigation of Li^+ coordination environments and diffusion mechanisms were performed using *ab initio* molecular dynamics simulations (AIMD)[47] and static DFT thermochemical computations. Such methods have been successfully employed for investigating the effect of Li^+ microenvironment in other solid-state electrolytes including polyethylene oxide (PEO)[44] and $La_3Li_7Zr_2O_{12}$ garnet (LLZO),[44] as well as aprotic organic solvents including dimethyl sulfoxide (DMSO) and acetonitrile (CH_3CN).[48,49]

Fig. 4 shows sequential Li^+ coordination environments within four-fold and three-fold coordination environments, which were identified from a series of AIMD equilibration calculations starting from a variety of initial configurations. These identified Li^+ coordinated structures were further analyzed by performing structural relaxations using static DFT calculations to further isolate stable states during the rotation, ligand dissociation, and association processes, all involved in Li^+ transport in [AdImMe][TFSI]. The calculated free energy profile with the respective atomic-scale insets along the transport coordinate (see Fig. 4) illustrates a plausible Li^+ transport pathway in [AdImMe][TFSI] at the atomic level.

As shown in Fig. 4, the ground state of Li^+ is a tetrahedrally coordinated shell with four O atoms from three TFSI anions, where the bottom TFSI ligand adopts a bidentate configuration. Notably, we also examined other potential Li^+ solvation scenarios, involving coordinating sites with F, N, C, S, and/or H atoms belonging to the TFSI. However, none of these

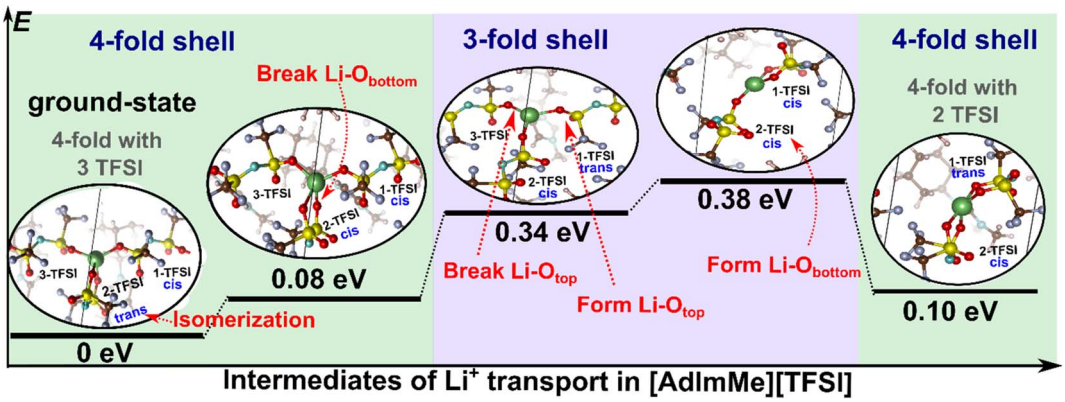

Fig. 4 Energy diagram for Li^+ transport in [AdImMe][TFSI] from a series of AIMD equilibration calculations. Insets show ball-and-stick structures of AIMD-determined Li coordination environments in [AdImMe][TFSI]. Sequential insets show the migration of Li through [AdImMe][TFSI] along the lowest energy Li transport pathway. Red arrows denote the structural changes between subsequent steps. Alternative pathways are included in SI Fig. S2. All energies are referenced to the ground state energy. The following color scheme was used for atoms: Li – green, O – red, S – yellow, C – brown, N – dark grey, F – teal, H – light pink.

coordination sites remained stable within the Li^+ shell after 3 ps of AIMD equilibration. During this equilibration time, significant structural reorganization occurred spontaneously, leading Li^+ bonding to oxygen atoms. Starting from this ground-state configuration (with its DFT energy set to 0 eV in Fig. 4), we found that Li^+ transport initiates through the isomerization of a bidentate TFSI anion from *trans* to *cis* by overcoming a small thermochemical barrier of 0.08 eV (7.9 kJ mol^{-1}). Subsequently, one of the Li–O bonds in the *cis*-bidentate TFSI ligand can be broken, leading to a state that is 0.34 eV (33.4 kJ mol^{-1}) above the ground state. As a result, the coordination shell of Li^+ transforms from a four-fold to a three-fold intermediate but retains three TFSI ligands.

The stable minimum with the highest energy (0.38 eV) (37.4 kJ mol^{-1}) is the result of two ligand dissociation and association reactions. Namely, one TFSI ligand (labeled as 3-TFSI) is released, while another TFSI (labeled as 1-TFSI) rotates to provide bidentate O coordination enabling a Li^+ solvation shell in a three-fold coordination environment. Furthermore, through AIMD simulations, we confirmed the instability of two-fold coordination shells involving two TFSI anions, indicating no additional stable intermediates exist between the two states within the three-fold shell shown in Fig. 4. During a brief 3 ps equilibration, all two-fold configurations we tried as initial guesses were found to spontaneously reorganize into one of the three-fold configurations observed in Fig. 4. In a subsequent step, the highest energy minimum (0.38 eV) releases 0.28 eV (27.5 kJ mol^{-1}) with the triangular Li^+ shell attracting one more O site from the bottom TFSI anion (labeled as 2-TFSI) to form a square four-fold shell with two bidentate-coordinated TFSI ligands (state labeled with +0.10 eV in Fig. 4). This state represents a symmetrical midpoint in the diffusion path across the unit cell whereby a symmetric reverse path can be followed to arrive at the initial ground state. Accordingly, the Li^+ charge carrier has completed its two-dimensional transport pathway from the unit cell boundary to the center of the crystalline [AdImMe][TFSI] unit cell. Snapshots of Li^+ diffusion within the full unit cell from the ground state to the center of the unit cell are shown in SI Fig. S1.

The pathway discussed above represents the thermochemically most favorable pathway for two-dimensional Li^+ transport in [AdImMe][TFSI] where the elimination of one TFSI ligand step is the thermochemical potential determining step, corresponding to a 0.38 eV increase from the ground state. The energetics of that step is comparable to that (0.2–0.3 eV) of other popular but expensive solid-state transition metal oxide electrolytes and electrodes.[43–45] However, we note that our computations are purely thermochemical estimates and therefore represent a lower bound in energy barriers for Li^+ transport in this material. Furthermore, the potential determining step undergoes a two-step preparatory process of isomerization and a transformation of one TFSI ligand from bidentate to monodentate coordination. Without these preceding steps, TFSI elimination becomes much more thermochemically unfavorable with an energy increase of 0.50 eV and 0.85 eV from the ground state, respectively (SI Fig. S2). Overall, our observations of the configurational transformations in the Li coordination environment with TFSI ligands provide valuable insights into the mechanisms of Li^+ transport in these solid-state organic electrolytes featuring diamondoid salts.

Discussion

Ionic electrolytes have shown promise, but do not demonstrate lithium transference necessary to compete with carbonate electrolytes. The diamondoid electrolytes we investigated here show similar conductivities at elevated temperatures as ionic liquids or organic ionic plastic crystals. An important distinction is that pure ionic liquids and organic ionic plastic crystals are conductive while neat diamondoid electrolytes are electrical insulators. The significant rise in conductivity of diamondoid salts upon addition of lithium cations indicates that diamondoid electrolytes are likely lithium single-ion conductors, which is consistent with the findings of our DFT computations.

While only one of the three diamondoid electrolytes evaluated shows promise for batteries operating at modestly elevated temperatures, this set of electrolytes shows how TFSI conformation impacts conductivity. Previously, we had analyzed ^{7}Li spectra to determine that the *gauche* conformer in the [AdImMe][TFSI] electrolyte likely results in higher lithium mobility than diamantyl-substituted cations.[23] Raman and ^{19}F NMR spectra suggest that TFSI does not exist in a *gauche* conformation in the Diam-1-ImMe or Diam-4-ImMe containing electrolyte. The presence of *cis* or *trans* conformers in these cases results in solvated lithium cations that are less mobile, as observed in EIS measurements conducted at 75 °C.

Differences in conformation and electron density in the TFSI anions present in the [Diam-1-ImMe][TFSI] and [Diam-4-ImMe][TFSI] salts appear to have minimal influence on the measured conductivity of mixtures with [Li][TFSI] at elevated temperatures (SI Fig. S3 and S4). Our DFT computations demonstrate that in mixtures of [Li][TFSI] and [AdImMe][TFSI], multiple TFSI conformers may exist that differ from those observed in neat [AdImMe][TFSI] as illustrated in Fig. 4. Extending this observation to the [Diam-1-ImMe][TFSI] and [Diam-4-ImMe][TFSI] salts, the TFSI anion could exist in both *cis* and *trans* conformers in mixtures of either salt with [Li][TFSI]. We hypothesize that multiple *cis* conformers exist in the [Diam-1-ImMe][TFSI] salt, but the existence of multiple conformers likely does not prevent bidentate coordination of TFSI to lithium ions.

As the concentration of [Li][TFSI] in [AdImMe][TFSI] increases so does the conductivity we measured for these electrolytes. Within the concentration range evaluated, this trend is not linear, and the conductivity increases by almost an order of magnitude with each five percent increase in the total mole percent of [Li][TFSI]. To the best of our knowledge, no other class of material experiences such a significant increase in conductivity as a function of concentration. We hypothesize that this increased conductivity is related to the number of active sites available for lithium transport, which increases with the number of charge carriers. A full investigation of why conductivity is so sensitive to both temperature and lithium concentration will be the subject of future work.

We also find that as the lithium concentration in [AdImMe][TFSI] increases, the salt becomes more physically malleable. While malleability conventionally indicates mobility of ions other than lithium in systems like organic ionic plastic crystals,[38,50] our datum suggests that adamantane-templated assembly inhibits organic cation mobility. Solid-state ^{13}C NMR data of [AdImMe][TFSI] and [Li][TFSI] mixtures published previously[23] does not change with [Li][TFSI] concentration, which indicates that the cationic "backbone" remains intact and AdImMe transport is unlikely. PFG NMR measurements further support this, as the hydrogen self-diffusion coefficient is below the measurable limits, implying that AdImMe is essentially immobile.

In contrast, the fluorine self-diffusion coefficient closely follows that of lithium across increasing temperatures. The agreement between the lithium and fluorine diffusion coefficients can indicate that coordinated transport of Li and TFSI occurs within dynamic TFSI channels. Additionally, TFSI anions are well known to undergo conformational changes between *cis*- and *trans*-isomers in the solid state, which could also result in a portion of the measured TFSI diffusion coefficient, as conformational fluctuations may appear as translational motion, limiting our ability to make definitive conclusions about TFSI motion based solely on the diffusion data we collected.

While we cannot conclusively determine how the measured TFSI mobility is distributed between conformational and translational degrees of freedom, we note that the activation energy for lithium mobility measured with PFG NMR (0.32 eV) is in quantitative agreement with the activation energy for lithium transport calculated *via* DFT (0.38 eV). Our DFT computations predict the lithium transport mechanism between coordination sites formed by a TFSI network, which is typically the mechanism associated with ion hopping. Thus, comparable activation energies obtained from both DFT and PFG NMR suggest that lithium conduction is linked to lithium hopping where only lithium ions are mobile.

Further, EIS measurements rule out the presence of a secondary mechanism for ionic motion that is similar in conductivity to what we observe with lithium (SI Fig. S5). Other electrolytes demonstrate pure blocking behavior at low frequencies[51] while diamondoid electrolytes show diffusion-limiting behavior. The magnitude of resistance indicates that any other ionic conduction would be orders of magnitude lower than what we observe with lithium. Therefore, although our findings are consistent with a single-ion conducting electrolyte, further investigation is needed to fully validate this hypothesis. Nonetheless, the current data are sufficient to conclude that the adamantane-templated electrolyte functions as a single-cation conductor.

Finally, there is deviation between the experimental apparent activation energy obtained from EIS (0.93 eV–1.24 eV) and those determined by DFT (0.38 eV) and PFG NMR (0.32 eV). As noted previously, only the thermochemistry of elementary steps involved in Li^+ transport were considered, and therefore, DFT data represent a lower bound on the energy barriers for Li^+ transport in this material. Similarly, PFG NMR probes length scales comparable to those in DFT calculations and neglects additional impedances that may be associated with defects, such as grain boundaries or interfacial impedances.

Long range transport of lithium within electrolytes will involve ion conduction through regions where increased impedance is expected, such as transporting lithium through grain boundaries, which leads to the higher calculated apparent activation energy values obtained from EIS. Additionally, our DFT computations show that changes in TFSI conformation play a key role in lowering the lithium transport activation energy from 0.85 eV down to 0.38 eV. Hence, the measured activation energies of 1 eV could also indicate that lithium mobility in the diamondoid electrolyte is occurring without associated anion conformational changes that lower activation energies in DFT computations. Therefore, DFT values are likely to be representative of electrolytes where morphology is optimized to promote lithium mobility and suggest that additional

work towards modifying materials processing conditions may provide further opportunities for increasing the conductivity of diamondoid electrolytes.

Conclusion

We demonstrate that adamantane and diamantane moieties can be used to promote single lithium-cation conduction in diamondoid-derived electrolytes. By leveraging dispersion interactions and packing mismatches, we find that diamondoid-imidazolium cations can template TFSI anions into lithium conduction networks. We find that [AdImMe][TFSI] has elevated temperature conductivity that is competitive with other solid electrolytes upon adding [Li][TFSI]. Further, increases in the concentration of [Li][TFSI] result in order-of-magnitude increases in the conductivity of the material across a large temperature range. First-principles calculations and AIMD simulations support a two-dimensional lithium-ion transport pathway through the bulk material where the lowest energy state is four-coordinated involving three anions. The mechanistic insights of Li^+ transport in the solid-state [AdImMe][TFSI] electrolyte highlight the key role of configurational transformations within Li coordination environments, particularly the elimination and isomerization processes, in enabling efficient Li^+ transport. These insights offer valuable guidance for understanding and optimizing ionic conductivity in such innovative solid-state organic electrolytes. Overall, this work motivates further exploration of diamondoid-derived electrolytes as a unique class of material where self-assembly of rigid non-polar diamondoid groups can be leveraged to template single lithium-cation conduction channels in solid organic salt electrolytes. We view these diamondoid-templated channels as a way to address challenges associated with low lithium transference in conventional ionic liquid and polymeric electrolytes.

Materials and methods

Synthesis and sample preparation

We have previously published the detailed synthesis of diamondoid salts[23] and methods for tuning the functionalization of diamondoid groups.[52] Mixtures of the diamondoid salts with [Li][TFSI] were prepared similar to previous studies,[23] where we melted the mixtures at 100 °C and dried for 48 hours.

NMR measurements

Solid-state NMR spectra were acquired on a Bruker Avance III spectrometer at a 11.74 T magnetic field strength ($\upsilon_0(^1H)$ = 500.22 MHz). Samples were packed in a glovebox into 4 mm zirconia NMR rotors with O-ring sealed Torlon caps. ^{19}F ($\upsilon_0(^{19}F)$ = 470.72 MHz) NMR spectra were acquired using a 3.5 μs 90° pulse length and a 10 kHz spinning speed. Spectra shown represent 64 signal average with a 0.05 s acquisition time and a 5 s recycle delay between scans.

Pulsed field gradient NMR

Pulsed field gradient (PFG) NMR experiments were performed on a Bruker AVANCE III 500 MHz spectrometer equipped with a 5 mm diffusion broadband (DiffBB) probe featuring a *z*-gradient coil capable of producing magnetic field gradients up to 53.5 G cm^{-1}. Samples were prepared in standard 5 mm NMR tubes in an argon glovebox. The sample temperature was varied from 22 to 70 °C. ^7Li spectra were acquired using a gradient pulse duration of 3 ms, a diffusion delay of 500 ms, and a repetition delay of 2 s. ^{19}F spectra were obtained with a gradient pulse duration of 1.9 ms, a diffusion delay of 560 ms, and a repetition delay of 1.5 s. The number of scans ranged from 2048 to 2560. All spectra were processed using the Mnova DOSY calculation. Phase and baseline were manually corrected.

Conductivity measurements

Mixtures of [Li][TFSI] and diamondoid salt were created by melting the mixtures at 100 °C and holding at reduced pressure for 2 days. Mixtures were solidified near their melting points and kept in an argon glovebox. 6 mm diameter pellets of the mixtures were formed at a pressure of 16 MPa. Copper discs of 6 mm diameter and 0.1 mm thickness were pressed on either side of the pellet as it was formed. Prior to pellet pressing, the oxide layer on the copper was removed using acetic acid as described by Chavez *et al.*[53] After oxide removal the copper was stored in an argon filled glovebox.

The pellets of salt sandwiched by copper were placed into pouch cells. These cells were constructed using nickel electrodes, stainless steel shims on either side of the pellet, and plastic spacers between the shims and around the pellet. The pouches were vacuum sealed in an argon glovebox. The pouches were approximately 7.6 cm by 5.0 cm in size. Before running EIS, the cells are heated to 60 °C for 1 h to anneal the electrolyte to the copper electrodes.

The conductivity was evaluated using EIS. We collected the impedance of the pellets by applying an oscillating sine wave of 256 mV amplitude over a 100 kHz to 1 Hz frequency range. Ten data points were collected every decade for a total of 51 data points. No potential was applied, and all measurements were taken at the open circuit potential. This data was fitted using an equivalent circuit model shown in Fig. 5 including three resistors (R1, R2, and R3) and two constant phase elements (Q2 and Q3).

Computational details

To identify plausible Li^+ diffusion pathways, we adopted a two-step approach. First, *ab initio* molecular dynamics (AIMD)[47] was

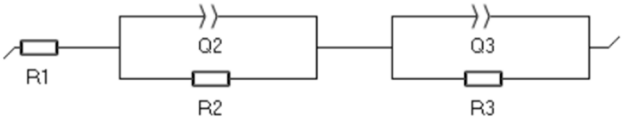

Fig. 5 Equivalent circuit model used to calculate conductivity. R2 represents the resistance to ionic conductivity.

used to screen stable coordination environments based on a series of initial configurations. For stable coordination environments identified *via* AIMD, additional static density functional theory (DFT) optimizations were performed to obtain final refined structures and energetics. To simulate Li^+ additions, one $[AdImMe]^+$ was replaced with one Li^+ cation in the unit cell of [AdImMe][TFSI] with a total of four cation–anion pairs, thus simulating a molar concentration of $c(Li^+) = 0.25$. Unit cell information is provided in Table S1.

All DFT computations were performed using the Vienna *Ab Initio* Simulation Package[54,55] within the projector-augmented wave approach.[56] Generalized gradient approximation utilizing the revised Perdew–Burke–Ernzerhof (PBE) exchange–correlation functional[57] was employed and corrected for long-range dispersion interactions using a nonlocal vdW-DF functional.[58] For static optimizations, a cutoff energy of 600 eV was chosen, and the convergence criteria for the total energy and atomic forces were set to 10^{-6} eV and 0.02 eV $Å^{-1}$, respectively. A $3 \times 3 \times 1$ Monkhorst–Pack *k*-point mesh was used for all static DFT computations.[59]

Born-Oppenheimer molecular dynamics (BOMD) method was employed to equilibrate different initial microenvironments of Li^+ in [AdImMe][TFSI] for 3 ps using a time step $t = 1$ fs. The Nose–Hoover thermostat[60,61] was used to keep the BOMD simulation temperature around 300 K. The obtained Li^+ coordination shells with stability at 300 K are shown in Fig. 4 and S2.

Conflicts of interest

The authors declare the following competing financial interest(s): composition of matter patent filed on diamondoid-derived salts.

Data availability

The data supporting this article have been included as part of the SI. Supplementary information: additional electrochemical characterization data, optical spectroscopy data, nuclear magnetic resonance spectroscopy data, density functional theory computational data, and images of electrochemical cells. See DOI: **https://doi.org/10.1039/d5ta03373j**.

Acknowledgements

Research was sponsored by the Army Research Office and was accomplished under Grant Number W911NF-23-1-0001. The views and conclusions contained in this document are those of the authors and should not be interpreted as representing the official policies, either expressed or implied, of the Army Research Office or the U.S. Government. The U.S. Government is authorized to reproduce and distribute reprints for Government purposes notwithstanding any copyright notation herein. A generous gift from Paul J. and Margaret M. Bender enabled the Bruker Avance III 500 to be purchased and the UW2020 fund enabled adding solid state NMR capability to this spectrometer in 2017. Hrishikesh Tupkar acknowledges support from the Department of Defense (DoD) through the National Defense Science and Engineering Graduate Fellowship (NDSEG). Computational work was supported by the US Department of Energy, Basic Energy Sciences (DOE-BES), Division of Chemical Sciences, Catalysis Science Program, grant number DE-FG02-05ER15731. We used resources at the National Energy Research Scientific Computing Center, a DOE Office of Science User Facility supported by the Office of Science of the US Department of Energy under contract no. DE-AC02-05CH11231 using NERSC award number BES-ERCAP0032205, and the UW-Madison's Center for High Throughput Computing (CHTC). The CHTC is supported by the University of Wisconsin-Madison, the Advanced Computing Initiative, the Wisconsin Alumni Foundation, the Wisconsin Institute for Discovery, and the National Science Foundation. We thank Dr Nicole Kruse from Bruker Biospin (Billerica, MA) for PFG diffusion measurements.

References

1 G. G. Eshetu, *et al.*, Fire behavior of carbonates-based electrolytes used in Li-ion rechargeable batteries with a focus on the role of the $LiPF_6$ and LiFSI salts, *J. Power Sources*, 2014, **269**, 804–811, DOI: **10.1016/j.jpowsour.2014.07.065**.

2 X. Q. Zhu, *et al.*, Overcharge investigation of large format lithium-ion pouch cells with $Li(Ni_{0.6}Co_{0.2}Mn_{0.2})O_2$ cathode for electric vehicles: Thermal runaway features and safety management method, *Energy*, 2019, **169**, 868–880, DOI: **10.1016/j.energy.2018.12.041**.

3 A. Eftekhari, Y. Liu and P. Chen, Different roles of ionic liquids in lithium batteries, *J. Power Sources*, 2016, **334**, 221–239, DOI: **10.1016/j.jpowsour.2016.10.025**.

4 X. Tang, S. Y. Lv, K. Jiang, G. H. Zhou and X. M. Liu, Recent development of ionic liquid-based electrolytes in lithium-ion batteries, *J. Power Sources*, 2022, **542**, 231792, DOI: **10.1016/j.jpowsour.2022.231792**.

5 X. E. Wang, *et al.*, Toward High-Energy-Density Lithium Metal Batteries: Opportunities and Challenges for Solid Organic Electrolytes, *Adv. Mater.*, 2020, **32**, 1905219, DOI: **10.1002/adma.201905219**.

6 M. Galinski, A. Lewandowski and I. Stepniak, Ionic liquids as electrolytes, *Electrochim. Acta*, 2006, **51**, 5567–5580, DOI: **10.1016/j.electacta.2006.03.016**.

7 A. Jarosik, S. R. Krajewski, A. Lewandowski and P. Radzimski, Conductivity of ionic liquids in mixtures, *J. Mol. Liq.*, 2006, **123**, 43–50, DOI: **10.1016/j.molliq.2005.06.001**.

8 L. Y. Jin, *et al.*, An organic ionic plastic crystal electrolyte for rate capability and stability of ambient temperature lithium batteries, *Energy Environ. Sci.*, 2014, **7**, 3352–3361, DOI: **10.1039/c4ee01085j**.

9 Y. S. Meng, V. Srinivasan and K. Xu, Designing better electrolytes, *Science*, 2022, **378**, 1065, DOI: **10.1126/science.abq3750**.

10 H. Park, C. Bin Park and B. J. Sung, The effects of defects on the transport mechanisms of lithium ions in organic ionic

plastic crystals, *Phys. Chem. Chem. Phys.*, 2023, **25**, 23058–23068, DOI: 10.1039/d3cp02088f.

11 T. Frömling, M. Kunze, M. Schönhoff, J. Sundermeyer and B. Roling, Enhanced Lithium Transference Numbers in Ionic Liquid Electrolytes, *J. Phys. Chem. B*, 2008, **112**, 12985–12990, DOI: 10.1021/jp804097j.

12 A. Fernicola, F. Croce, B. Scrosati, T. Watanabe and H. Ohno, LiTFSI-BEPyTFSI as an improved ionic liquid electrolyte for rechargeable lithium batteries, *J. Power Sources*, 2007, **174**, 342–348, DOI: 10.1016/j.jpowsour.2007.09.013.

13 M. Gouverneur, F. Schmidt and M. Schönhoff, Negative effective Li transference numbers in Li salt/ionic liquid mixtures: does Li drift in the "Wrong" direction?, *Phys. Chem. Chem. Phys.*, 2018, **20**, 7470–7478, DOI: 10.1039/c7cp08580j.

14 L. Aguilera, J. Völkner, A. Labrador and A. Matic, The effect of lithium salt doping on the nanostructure of ionic liquids, *Phys. Chem. Chem. Phys.*, 2015, **17**, 27082–27087, DOI: 10.1039/c5cp03825a.

15 Z. P. Rosol, N. J. German and S. M. Gross, Solubility, ionic conductivity and viscosity of lithium salts in room temperature ionic liquids, *Green Chem.*, 2009, **11**, 1453–1457, DOI: 10.1039/b818176d.

16 J. Asenbauer, N. Ben Hassen, B. D. McCloskey and J. M. Prausnitz, Solubilities and ionic conductivities of ionic liquids containing lithium salts, *Electrochim. Acta*, 2017, **247**, 1038–1043, DOI: 10.1016/j.electacta.2017.07.053.

17 S. Seki, *et al.*, Imidazolium-based room-temperature ionic liquid for lithium secondary batteries - Effects of lithium salt concentration, *J. Electrochem. Soc.*, 2007, **154**, A173–A177, DOI: 10.1149/1.2426871.

18 M. L. P. Le, *et al.*, Structure-Properties Relationships of Lithium Electrolytes Based on Ionic Liquid, *J. Phys. Chem. B*, 2010, **114**, 894–903, DOI: 10.1021/jp9098842.

19 A. Martinelli, *et al.*, Phase Behavior and Ionic Conductivity in Lithium Bis(trifluoromethanesulfonyl)imide-Doped Ionic Liquids of the Pyrrolidinium Cation and Bis(trifluoromethanesulfonyl)imide Anion, *J. Phys. Chem. B*, 2009, **113**, 11247–11251, DOI: 10.1021/jp905783t.

20 V. Lesch, Z. Li, D. Bedrov, O. Borodin and A. Heuer, The influence of cations on lithium ion coordination and transport in ionic liquid electrolytes: a MD simulation study, *Phys. Chem. Chem. Phys.*, 2016, **18**, 382–392, DOI: 10.1039/c5cp05111h.

21 J. P. Wagner and P. R. Schreiner, London Dispersion in Molecular Chemistry-Reconsidering Steric Effects, *Angew. Chem., Int. Ed.*, 2015, **54**, 12274–12296, DOI: 10.1002/anie.201503476.

22 L. Rummel and P. R. Schreiner, Advances and Prospects in Understanding London Dispersion Interactions in Molecular Chemistry, *Angew. Chem., Int. Ed.*, 2024, **63**, 202316364, DOI: 10.1002/anie.202316364.

23 J. McAlpine, *et al.*, Modulating Entropic Driving Forces to Promote High Lithium Mobility in Solid Organic Electrolytes, *Chem. Mater.*, 2023, **35**, 3545–3554, DOI: 10.1021/acs.chemmater.3c00141.

24 A. A. Fokin, M. Šekutor and P. R. Schreiner, *The Chemistry of Diamondoids: Building Blocks for Ligands, Catalysts, Materials, and Pharmaceuticals*, Wiley-VCH, 2024, ISBN: 978-3-527-34391-1.

25 H. Schwertfeger, A. A. Fokin and P. R. Schreiner, Diamonds are a chemist's best friend: Diamondoid chemistry beyond adamantane, *Angew. Chem., Int. Ed.*, 2008, **47**, 1022–1036, DOI: 10.1002/anie.200701684.

26 A. A. Fokin, *et al.*, Stable Alkanes Containing Very Long Carbon-Carbon Bonds, *J. Am. Chem. Soc.*, 2012, **134**, 13641–13650, DOI: 10.1021/ja302258q.

27 E. M. King, M. A. Gebbie and N. A. Melosh, Impact of Rigidity on Molecular Self-Assembly, *Langmuir*, 2019, **35**, 16062–16069, DOI: 10.1021/acs.langmuir.9b01824.

28 S. Rösel, J. Becker, W. D. Allen and P. R. Schreiner, Probing the Delicate Balance between Pauli Repulsion and London Dispersion with Triphenylmethyl Derivatives, *J. Am. Chem. Soc.*, 2018, **140**, 14421–14432, DOI: 10.1021/jacs.8b09145.

29 P. R. Schreiner, *et al.*, Overcoming lability of extremely long alkane carbon-carbon bonds through dispersion forces, *Nature*, 2011, **477**, 308–311, DOI: 10.1038/nature10367.

30 F. Philippi, *et al.*, Flexibility is the key to tuning the transport properties of fluorinated imide-based ionic liquids, *Chem. Sci.*, 2022, **13**, 9176–9190, DOI: 10.1039/d2sc03074h.

31 G. Veryasov, U. Harinaga, K. Matsumoto and R. Hagiwara, Crystallographic Insight into the Mg^{2+} Coordination Mode and $N(SO_2CF_3)_2^-$ Anion Conformation in $Mg[N(SO_2CF_3)_2]_2$ and Its Adducts, *Eur. J. Inorg. Chem.*, 2017, **1087–1099**, DOI: 10.1002/ejic.201601305.

32 J. L. Nowinski, P. Lightfoot and P. G. Bruce, Structure of $LiN(CF_3SO_2)_2$, a Novel Salt for Electrochemistry, *J. Mater. Chem.*, 1994, **4**, 1579–1580, DOI: 10.1039/jm9940401579.

33 K. Matsumoto, T. Matsui, T. Nohira and R. Hagiwara, Crystal structure of $Na[N(SO_2CF_3)_2]$ and coordination environment of alkali metal cation in the $M[N(SO_2CF_3)_2]$ ($M^+ = Li^+$, Na^+, K^+, and Cs^+) structures, *J. Fluorine Chem.*, 2015, **174**, 42–48, DOI: 10.1016/j.jfluchem.2014.07.021.

34 A. Martinelli, *et al.*, Conformational evolution of $TFSI^-$ in protic and aprotic ionic liquids, *J. Raman Spectrosc.*, 2011, **42**, 522–528, DOI: 10.1002/jrs.2713.

35 F. Castiglione, *et al.*, Pyrrolidinium-Based Ionic Liquids Doped with Lithium Salts: How Does Li^+ Coordination Affect Its Diffusivity?, *J. Phys. Chem. B*, 2014, **118**, 13679–13688, DOI: 10.1021/jp509387r.

36 J. C. Lassègues, J. Grondin, C. Aupetit and P. Johansson, Spectroscopic Identification of the Lithium Ion Transporting Species in LiTFSI-Doped Ionic Liquids, *J. Phys. Chem. A*, 2009, **113**, 305–314, DOI: 10.1021/jp806124w.

37 Y. Chen, *et al.*, Probing Conformational Evolution and Associated Dynamics of $Mg(N(SO_2CF_3)_2)_2$•Dimethoxyethane Adduct Using Solid-State ^{19}F and ^1H NMR, *J. Phys. Chem. C*, 2020, **124**, 4999–5008, DOI: 10.1021/acs.jpcc.9b10212.

38 H. J. Zhu, A. Grzelak, R. Yunis, J. Martín and M. Forsyth, Decoupled ion mobility in nano-confined ionic plastic crystal, *Mater Adv.*, 2020, **1**, 3398–3405, DOI: 10.1039/d0ma00778a.

39 Z. Li, *et al.*, Ionic Conduction in Polymer-Based Solid Electrolytes, *Adv. Sci.*, 2023, **10**, DOI: 10.1002/advs.202201718.
40 J. C. Bachman, *et al.*, Inorganic Solid-State Electrolytes for Lithium Batteries: Mechanisms and Properties Governing Ion Conduction, *Chem. Rev.*, 2016, **116**, 140–162, DOI: 10.1021/acs.chemrev.5b00563.
41 J. A. Dawson, P. Canepa, T. Famprikis, C. Masquelier and M. S. Islam, Atomic-Scale Influence of Grain Boundaries on Li-Ion Conduction in Solid Electrolytes for All-Solid-State Batteries (vol 140, pg 362, 2018), *J. Am. Chem. Soc.*, 2018, **140**, 7044, DOI: 10.1021/jacs.8b04915.
42 F. Castiglione, *et al.*, Molecular Environment and Enhanced Diffusivity of Li^+ Ions in Lithium-Salt-Doped Ionic Liquid Electrolytes, *J. Phys. Chem. Lett.*, 2011, **2**, 153–157, DOI: 10.1021/jz101516c.
43 H. Han, *et al.*, Li iontronics in single-crystalline T-Nb_2O_5 thin films with vertical ionic transport channels, *Nat. Mater.*, 2023, **22**, DOI: 10.1038/s41563-023-01612-2.
44 C. Shi, *et al.*, Revealing the mechanisms of lithium-ion transport and conduction in composite solid polymer electrolytes, *Cell Rep. Phys. Sci.*, 2023, **4**, DOI: 10.1016/j.xcrp.2023.101321.
45 P. Ranque, J. Zagórski, S. Devaraj, F. Aguesse and J. M. L. del Amo, Characterization of the interfacial Li-ion exchange process in a ceramic-polymer composite by solid state NMR, *J. Mater. Chem. A*, 2021, **9**, 17812–17820, DOI: 10.1039/d1ta03720j.
46 L. Porcarelli, *et al.*, Single-Ion Conducting Polymer Nanoparticles as Functional Fillers for Solid Electrolytes in Lithium Metal Batteries, *ACS Appl. Mater. Interfaces*, 2021, **13**, 54354–54362, DOI: 10.1021/acsami.1c15771.
47 B. W. J. Chen and M. Mavrikakis, Modeling the impact of structure and coverage on the reactivity of realistic heterogeneous catalysts, *Nat. Chem. Eng.*, 2025, **2**, 181–197, DOI: 10.1038/s44286-025-00179-w.
48 Z. Jiang and A. M. Rappe, Structure, Diffusion, and Stability of Lithium Salts in Aprotic Dimethyl Sulfoxide and Acetonitrile Electrolytes, *J. Phys. Chem. C*, 2022, **126**, 10266–10272, DOI: 10.1021/acs.jpcc.2c02174.
49 Z. Jiang and A. M. Rappe, Uncovering the Electrolyte-Dependent Transport Mechanism of LiO2 in Lithium-Oxygen Batteries, *J. Am. Chem. Soc.*, 2022, **144**, 22150–22158, DOI: 10.1021/jacs.2c09700.
50 H. Zhu, *et al.*, Structure and Ion Dynamics in Imidazolium-Based Protic Organic Ionic Plastic Crystals, *J. Phys. Chem. Lett.*, 2018, **9**, 3904–3909, DOI: 10.1021/acs.jpclett.8b01500.
51 E. Kazyak, *et al.*, Atomic layer deposition and first principles modeling of glassy Li_3BO_3-Li_2CO_3 electrolytes for solid-state Li metal batteries, *J. Mater. Chem. A*, 2018, **6**, 19425–19437, DOI: 10.1039/c8ta08761j.
52 T. Rander, *et al.*, Electronic structure tuning of diamondoids through functionalization, *J. Chem. Phys.*, 2013, **138**, DOI: 10.1063/1.4774268.
53 K. L. Chavez and D. W. Hess, A novel method of etching copper oxide using acetic acid, *J. Electrochem. Soc.*, 2001, **148**, G640–G643, DOI: 10.1149/1.1409400.
54 G. Kresse and J. Furthmuller, Efficiency of *ab initio* total energy calculations for metals and semiconductors using a plane-wave basis set, *Comput. Mater. Sci.*, 1996, **6**, 15–50, DOI: 10.1016/0927-0256(96)00008-0.
55 G. Kresse and J. Furthmuller, Efficient iterative schemes for *ab initio* total-energy calculations using a plane-wave basis set, *Phys. Rev. B: Condens. Matter Mater. Phys.*, 1996, **54**, 11169–11186, DOI: 10.1103/PhysRevB.54.11169.
56 P. E. Blochl, Projector Augmented-Wave Method, *Phys. Rev. B: Condens. Matter Mater. Phys.*, 1994, **50**, 17953–17979, DOI: 10.1103/PhysRevB.50.17953.
57 J. P. Perdew, K. Burke and M. Ernzerhof, Generalized gradient approximation made simple, *Phys. Rev. Lett.*, 1996, **77**, 3865–3868, DOI: 10.1103/PhysRevLett.77.3865.
58 M. Dion, H. Rydberg, E. Schröder, D. C. Langreth and B. I. Lundqvist, Van der Waals density functional for general geometries -: art. no. 246401, *Phys. Rev. Lett.*, 2004, **92**, DOI: 10.1103/PhysRevLett.92.246401.
59 H. J. Monkhorst and J. D. Pack, Special Points for Brillouin-Zone Integrations, *Phys. Rev. B: Condens. Matter Mater. Phys.*, 1976, **13**, 5188–5192, DOI: 10.1103/PhysRevB.13.5188.
60 S. Nose and M. L. Klein, Constant Pressure Molecular-Dynamics for Molecular-Systems, *Mol. Phys.*, 1983, **50**, 1055–1076, DOI: 10.1080/00268978300102851.
61 W. G. Hoover, Canonical Dynamics - Equilibrium Phase-Space Distributions, *Phys. Rev. A*, 1985, **31**, 1695–1697, DOI: 10.1103/PhysRevA.31.1695.

